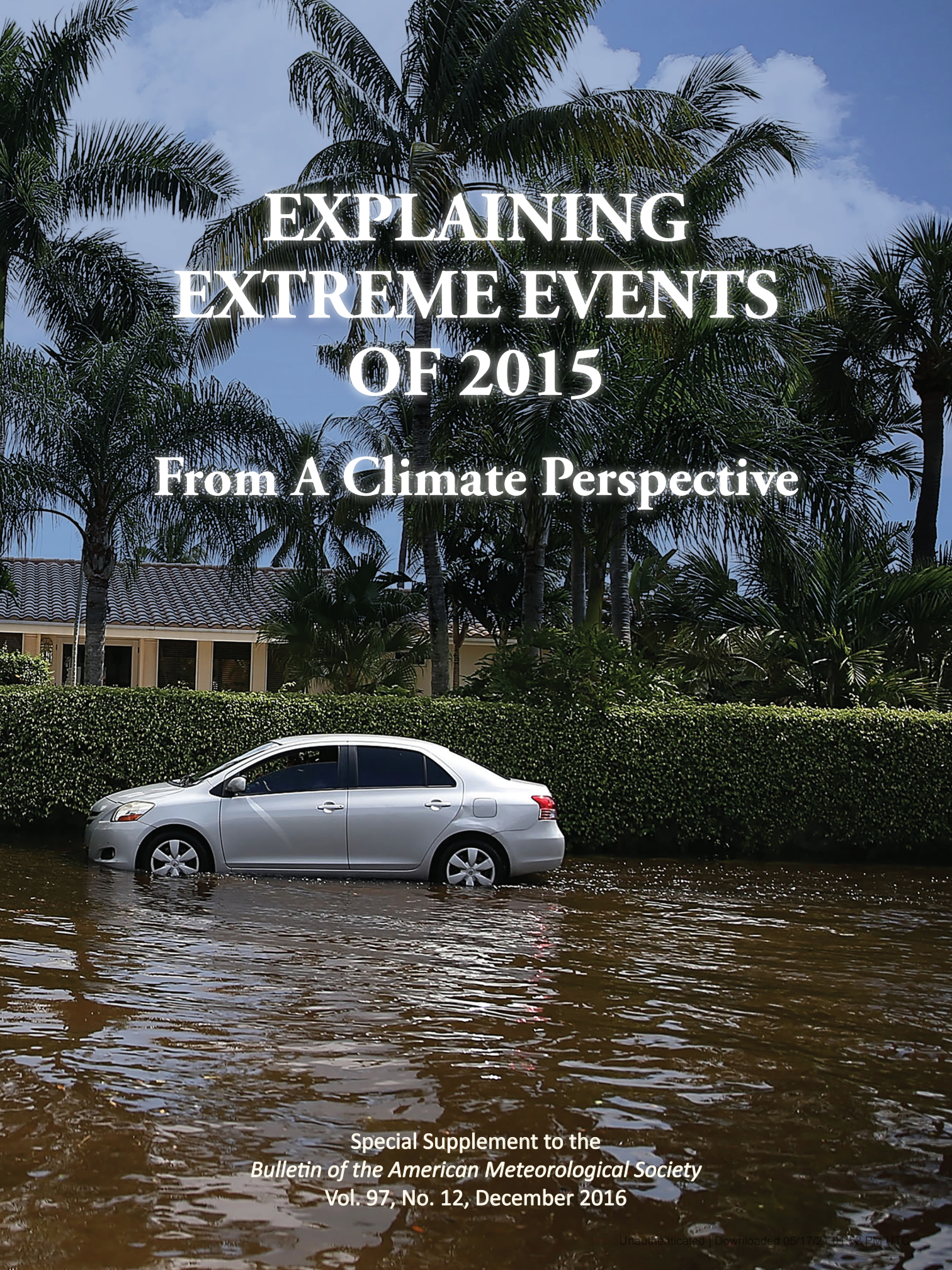

EXPLAINING EXTREME EVENTS OF 2015

From A Climate Perspective

Special Supplement to the
Bulletin of the American Meteorological Society
Vol. 97, No. 12, December 2016

EXPLAINING EXTREME EVENTS OF 2015 FROM A CLIMATE PERSPECTIVE

Editors

Stephanie C. Herring, Andrew Hoell, Martin P. Hoerling, James P. Kossin, Carl J. Schreck III, and Peter A. Stott

Special Supplement to the

Bulletin of the American Meteorological Society

Vol. 97, No. 12, December 2016

American Meteorological Society

Corresponding Editor:

Stephanie C. Herring, PhD
NOAA National Centers for Environmental Information
325 Broadway, E/CC23, Rm 1B-131
Boulder, CO, 80305-3328
E-mail: stephanie.herring@noaa.gov

Cover Credit:

©Photo by Joe Raedle/Getty Images—A vehicle drives through flooded streets caused by a combination of the lunar orbit which caused seasonal high tides and what many believe is the rising sea levels due to climate change on September 30, 2015, in Fort Lauderdale, Florida. South Florida is projected to continue to feel the effects of climate change, and many of the cities have begun programs such as installing pumps or building up sea walls to try and combat the rising oceans.

HOW TO CITE THIS DOCUMENT

Citing the complete report:

Herring, S. C., A. Hoell, M. P. Hoerling, J. P. Kossin, C. J. Schreck III, and P. A. Stott, Eds., 2016: Explaining Extreme Events of 2015 from a Climate Perspective. *Bull. Amer. Meteor. Soc.*, **97 (12)**, S1–S145.

Citing a section (example):

Partain, J. L., and Coauthors, 2016: An assessment of the role of anthropogenic climate change in the Alaska fire season of 2015 [in "Explaining Extremes of 2015 from a Climate Perspective"]. *Bull. Amer. Meteor. Soc.*, **97 (12)**, S14–S18, doi:10.1175/BAMS-D-16-0149.

EDITORIAL AND PRODUCTION TEAM

Riddle, Deborah B., Lead Graphics Production, NOAA/NESDIS National Centers for Environmental Information, Asheville, NC

Veasey, Sara W., Visual Communications Team Lead, NOAA/NESDIS National Centers for Environmental Information, Asheville, NC

Love-Brotak, S. Elizabeth, Graphics Support, NOAA/NESDIS National Centers for Environmental Information, Asheville, NC

Fulford, Jennifer, Editorial Support, Telesolv Consulting LLC, NOAA/NESDIS National Centers for Environmental Information, Asheville, NC

Griffin, Jessicca, Graphics Support, Cooperative Institute for Climate and Satellites-NC, North Carolina State University, Asheville, NC

Maycock, Tom, Editorial Support, Cooperative Institute for Climate and Satellites-NC, North Carolina State University, Asheville, NC

Misch, Deborah J., Graphics Support, Telesolv Consulting LLC, NOAA/NESDIS National Centers for Environmental Information, Asheville, NC

Osborne, Susan, Editorial Support, Telesolv Consulting LLC, NOAA/NESDIS National Centers for Environmental Information, Asheville, NC

Sprain, Mara, Editorial Support, LAC Group, NOAA/NESDIS National Centers for Environmental Information, Asheville, NC

Young, Teresa, Graphics Support, STG, Inc., NOAA/NESDIS National Centers for Environmental Information, Asheville, NC

TABLE OF CONTENTS

ABSTRACT—Stephanie C. Herring, Andrew Hoell, Martin P. Hoerling, James P. Kossin, Carl J. Schreck III, and Peter A. Stott

This fifth edition of explaining extreme events of the previous year (2015) from a climate perspective continues to provide evidence that climate change is altering some extreme event risk. Without exception, all the heat-related events studied in this year's report were found to have been made more intense or likely due to human-induced climate change, and this was discernible even for those events strongly influenced by the 2015 El Niño. Furthermore, many papers in this year's report demonstrate that attribution science is capable of separating the effects of natural drivers including the strong 2015 El Niño from the influences of long-term human-induced climate change.

Other event types investigated include cold winters, tropical cyclone activity, extreme sunshine in the United Kingdom, tidal flooding, precipitation, drought, reduced snowpack in the U.S. mountain west, arctic sea ice extent, and wildfires in Alaska. Two studies investigated extreme cold waves and monthly-mean cold conditions over eastern North America during 2015, and find these not to have been symptomatic of human-induced climate change. Instead, they find the cold conditions were caused primarily by internally generated natural variability. One of these studies shows winters are becoming warmer, less variable, with no increase in daily temperature extremes over the eastern United States. Tropical cyclone activity was extreme in 2015 in the western North Pacific (WNP) as measured by accumulated cyclone energy (ACE). In this report, a study finds that human-caused climate change largely increased the odds of this extreme cyclone activity season. The 2015 Alaska fire season burned the second largest number of acres since records began in 1940. Investigators find that human-induced climate change has increased the likelihood of a fire season of this severity.

Confidence in results and ability to quickly do an attribution analysis depend on the "three pillars" of event attribution: the quality of the observational record, the ability of models to simulate the event, and our understanding of the physical processes that drive the event and how they are being impacted by climate change. A result that does not find a role for climate change may be because one or more of these three elements is insufficient to draw a clear conclusion. As these pillars are strengthened for different event types, confidence in the presence and absence of a climate change influence will increase.

This year researchers also link how changes in extreme event risk impact human health and discomfort during heat waves, specifically by looking at the role of climate change on the wet bulb globe temperature during a deadly heat wave in Egypt. This report reflects a growing interest within the attribution community to connect attribution science to societal impacts to inform risk management through "impact attribution." Many will watch with great interest as this area of research evolves in the coming years.

2. MULTIMODEL ASSESSMENT OF ANTHROPOGENIC INFLUENCE ON RECORD GLOBAL AND REGIONAL WARMTH DURING 2015

Jonghun Kam, Thomas R. Knutson, Fanrong Zeng, and Andrew T. Wittenberg

In 2015, record warm surface temperatures were observed for the global mean, India, and the equatorial central Pacific. CMIP5 simulations suggest that for the globe and India, anthropogenic warming was largely to blame.

Introduction. HadCRUT4v4 observed surface temperature data (Morice et al. 2012; 5° × 5° lat.–lon. grid boxes) indicates that 2015 was a clear record-breaking year for global annual mean temperatures (Figs. 2.1a,b,e). In this analysis, we consider only grid boxes with at least 100 years of historical data, which narrows the focus mainly to the Atlantic and Indian Oceans, the North Pacific Ocean, Europe, the United States, southern Asia, and Australia (Fig. 2.1d). Sixteen percent of this analyzed area experienced record annual warmth during 2015 (Fig. 2.1d).

Observed global temperatures over the past decade had been warming at a rate less than the ensemble mean warming in the Coupled Model Intercomparison Project phase 5 all-forcing historical runs (CMIP5–ALL; Taylor et al. 2012). However, the record global temperature of 2015 (Fig. 2.1e), including the influence of a strong El Niño event (Fig. 2.1f), was warmer globally than the mean of the CMIP5-ALL model ensemble levels for 2015, relative to their respective 1881–1920 means.

Major regions with unprecedented annual mean warmth in 2015 included the northeast Pacific and northwest Atlantic, while during September–November (SON) 2015, southern India/Sri Lanka stood out with record seasonal warmth (Fig. 2.1g; our region of focus in southern India and Sri Lanka does include some SST influence, as we used the combined SST/Tair dataset; see Supplemental Material). Only a small region south of Greenland (0.2% of the globe) experienced record annual mean cold surface temperatures (Fig. 2.1d).

We constructed our regions of focus based on areas highlighted in Fig. 2.1d. These regions had some irregular shapes and were constructed to be mostly covered by new record annual or seasonal temperatures in 2015. In addition to global mean temperatures, we focused on two main regions and temporal domains—the Niño-4 region (annual means) and a region including southern India and Sri Lanka (SON means). To demonstrate the robustness for annual mean record warmth in 2015 over the Niño-4 region (Fig. 2.1g), we also showed extended reconstructed sea surface temperature (ERSST.v4; Huang et al. 2016) and Hadley Centre sea ice and sea surface temperature (HadISST1.1; Rayner et al. 2003) data reconstructions and found that these also show unprecedented annual mean warmth during 2015.

This study investigates the causes of these record warm events using an eight-model set of all-forcing (anthropogenic + natural) historical climate model runs, associated long-term control (unforced) runs, and natural forcing runs (CMIP5–ALL, –CONT, and –NAT, respectively). These eight models (listed in Supplemental Material) were selected, as they were the ones with CMIP5-NAT runs extending to 2012. Our methods follow the studies of Knutson et al. (2013 and 2014); some of the descriptive text below is drawn from those reports.

Time-evolving trend analyses for long-term global and regional anthropogenic warming. Figures 2.2a–c show analyses for long-term global and regional trends using different start years, but with a common end year (2012 for CMIP5–NAT and 2015 for CMIP5–ALL; the latter are extended with simulations forced by the RCP4.5 emissions scenario). Observed trends ending in 2012 and 2015 are shown for comparison.

AFFILIATIONS: Kam—NOAA/Geophysical Fluid Dynamics Laboratory and the Cooperative Institute for Climate Science, Princeton University, Princeton, New Jersey; Knutson, Zeng, and Wittenberg—NOAA/Geophysical Fluid Dynamics Laboratory, Princeton, New Jersey.

DOI:10.1175/BAMS-D-16-0138.1

A supplement to this article is available online (10.1175/BAMS-D-16-0138.2)

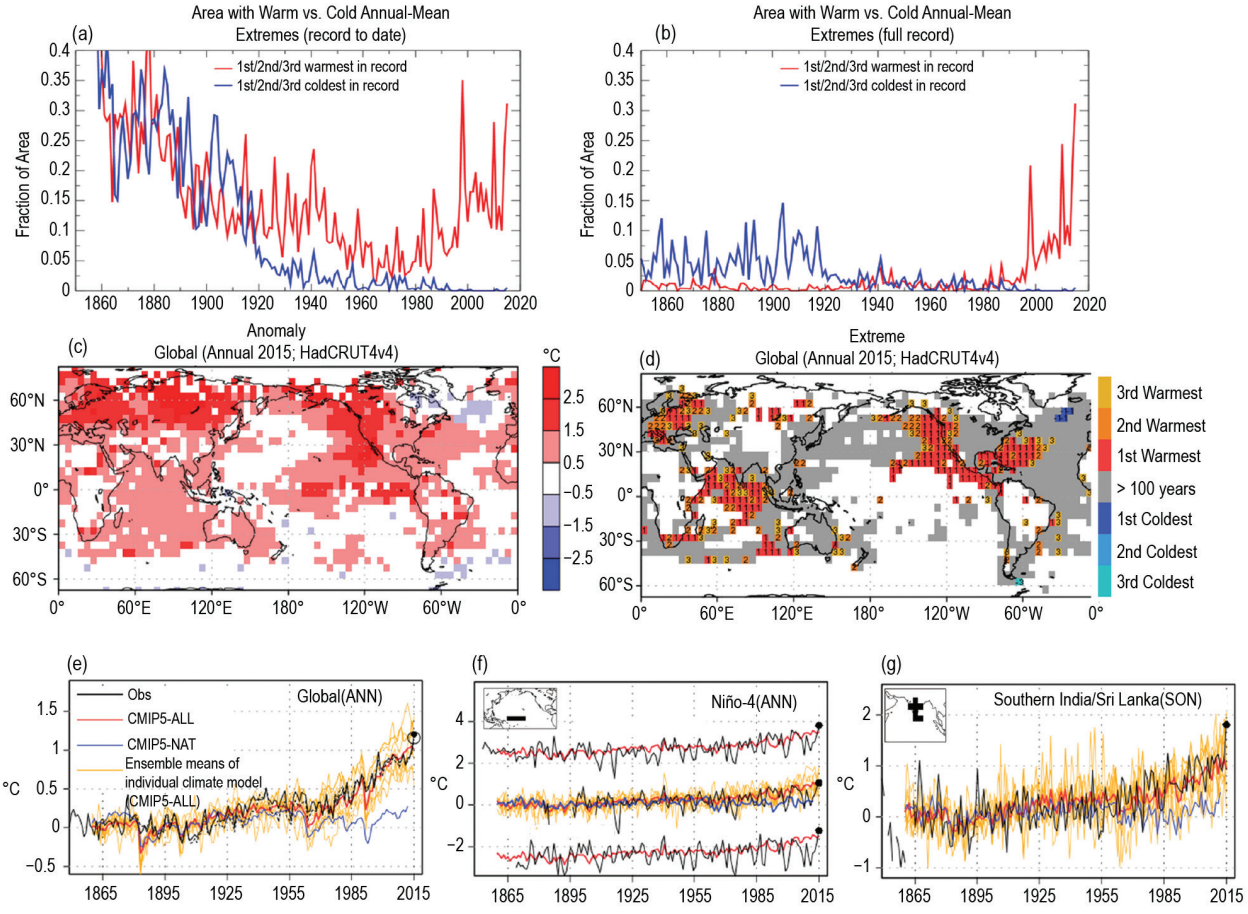

Fig. 2.1. (a),(b) Annual time series of the fractions of available global area with the top three warmest (red curve) and coldest (blue curve) annual mean temperatures in the available record (a) to that date and (b) to the entire record through 2015. (c) Annual mean surface air temperature anomalies (°C) for 2015 (relative to the 1961–90 base period) from the HadCRUT4v4 dataset. (d) Colors identify grid boxes with annual mean anomalies that rank 1st (dark red), 2nd (orange-red), or 3rd (yellow-orange) warmest in the available observed record. Only colored and gray areas have sufficiently long records, defined here as containing at least 100 available annual means, which require at least four available months. (e)–(g) Annual mean surface temperature anomalies (°C) for the globe, Niño-4 region, and southern India/Sri Lanka (SON). Red (CMIP5–ALL) and blue (CMIP5–NAT) curves indicate ensemble mean simulated anomalies through 2015 and 2012, respectively, with each available model weighted equally; orange curves indicate individual CMIP5–ALL ensemble members. Black curves indicate observed estimates from HadCRUT4v4 (solid) and NOAA NCEI (dotted). All time series are adjusted to have zero mean over the period 1881–1920. For the Niño-4 region, alternative observed anomalies from the ERSST.v4 and HadISST1.1 reconstructions and the ensemble anomalies for CMIP5–ALL are shown with +2.5°C and −2.5°C offsets from zero for display purposes.

For the sliding trends, we require at least 33% areal coverage in the region for at least the start year of the trend (Knutson et al. 2013), resulting in the gaps shown. The global mean analysis shows a pronounced observed warming, consistent with CMIP5–ALL yet statistically distinct from CMIP5–NAT, for all start years before about 1990. While the CMIP5–ALL runs occasionally are inconsistent with observed global trends through 2012 (at least for recent trends beginning in the 1990s), now that the record has been extended to 2015, we find that CMIP5–ALL trends beginning in the late 1990s now are generally consistent with observations.

For the Niño-4 region (Fig. 2.2b), we compare results from three different observational datasets. The ERSST.v4 shows the strongest indication of a detectable warming, consistent with the CMIP5–ALL runs but inconsistent with the CMIP5–NAT runs for start years up to around 1960. In contrast, the HadISST1.1 estimated trends are hardly distinguishable from the CMIP5–NAT runs, and also inconsistent with the CMIP5–ALL runs through most of the period. The observed seasonal mean time series (SON)

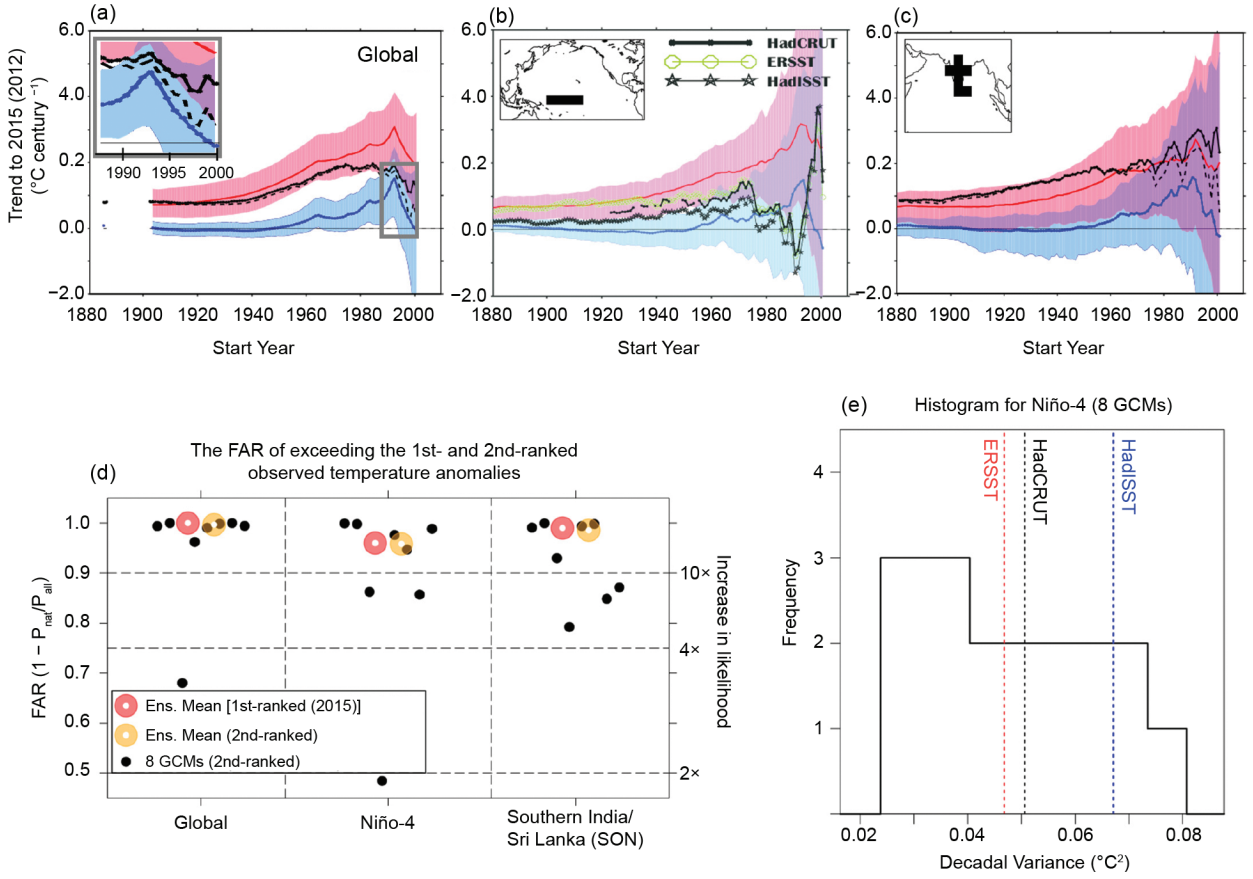

Fig. 2.2. (a)–(c) Sliding trends as a function of starting year, with ending year 2015 (black solid line) or 2012 (black dashed line) [°C (100 yr)$^{-1}$] for the globe, the Niño-4 region, and southern India/Sri Lanka. Black, red, and blue curves depict observations, CMIP5–ALL ensemble mean, and CMIP5–NAT ensemble mean, respectively. Black line/dots, green line/circles, and black line/stars depict observed trends from HadCRUT4, ERSST, and HadISST, respectively. Red (blue) lines depict the mean of trends from the CMIP5–ALL (CMIP5–NAT) runs, while pink (blue) bands depict the 5th–95th percentile range for an individual realization chosen randomly from the simulations, with equal representation for each model. Purple shading indicates the overlap of the pink and blue region. (d) Estimates of the FAR of exceeding the first- (2015) and second-ranked observed temperature anomaly thresholds from the CMIP5 multimodel ensemble (large red and orange circle, respectively); black solid circles correspond to the FAR estimated from the eight paired CMIP5–ALL and –NAT runs from individual CMIP5 models, for the second-ranked observed anomalies. (e) Histogram of the Niño-4 region variances for non-overlapping 155-year epochs of the eight individual model control runs, along with estimates from three observational datasets from which the model-estimated forced response has been removed (1861–2015).

over southern India/Sri Lanka (Fig. 2.2c) shows a pronounced warming, consistent with CMIP5–ALL regardless of trend start year, and detectable relative to CMIP5–NAT for start years up to the 1970s.

Overall, the trend analysis using the CMIP5 models shows a long-term warming over the globe and southern India/Sri Lanka (very likely attributable in part to anthropogenic forcing), and long-term trend results for the Niño-4 region that strongly depend on observational data uncertainties.

Model-based attributable risk assessment for the 2015 extreme warm anomalies. Considering the anomalies and new record-breaking temperatures in 2015, there are many regions that could have been selected for the fraction of attributable risk (FAR; Stott et al. 2004) analysis. The major regions of records include global, eastern Pacific, western Atlantic, Indian Ocean, Europe, and south of Greenland (cold record). For our report, we chose to compute the FAR for global temperature, the Niño-4 region (with the prominent El Niño in 2015), and southern India/Sri Lanka (SON). The FAR compares the event tail probabilities (P) between the CMIP5–NAT and CMIP5–ALL runs (FAR = 1 − P_{nat} / P_{all}). Forced responses are derived from the multimodel ensemble means of the

CMIP5–ALL and CMIP5–NAT simulations, while the impact of internal variability on the modeled trend distributions was estimated using the CMIP5–CONT runs (Knutson et al. 2013). Our FAR estimates use the first- (2015) and second-ranked observed positive anomaly as the extreme event thresholds (Fig. 2.2d). For extremely large anomalies, the FAR can be particularly difficult to estimate, as it is based on a ratio of very small areas under the distribution tails (Kam et al. 2015). Therefore we used the second-ranked observed anomalies as the threshold values for our primary FAR estimates, as these anomalies are not quite as extreme as the top-ranked ones.

According to the HadCRUT4v4, the second-ranked anomalies over the globe, southern India/Sri Lanka, and the Niño-4 region occurred in 2014, 2010, and 1888, respectively, while the ERSST.v4 and HadISST1.1 datasets show the second-ranked anomalies over the Niño-4 region occurred in different years (2002 and 1987, respectively). Based on the HadCRUT4v4, the simulated probabilities of exceeding the second-ranked anomalies for the globe, southern India/Sri Lanka, and the Niño-4 region are 58% (0.005%), 23% (0.3%), and 32% (1.5%) for the CMIP5–ALL (CMIP5–NAT) runs, respectively. Sensitivity tests for the Niño-4 region using the second-ranked anomalies from the ERSST.v4 and HadISST1.1 datasets are consistent with the results from the HadCRUT4v4 (not shown). The FAR estimates are 0.99, 0.98, and 0.95 for the globe, southern India/Sri Lanka (SON), and the Niño-4 regions, respectively. Uncertainties in the FAR estimates were explored by computing the spread of FAR estimates across individual CMIP5 models (Fig. 2.2d). These sensitivity tests show that, using the second-ranked year threshold values, the estimated FAR is above 0.9 for seven, five, and five out of eight individual models for the globe, Niño-4 region, and southern India/Sri Lanka, respectively (See Supplemental Material).

A crucial assumption of our study is that the internal variability simulated by the models represents the real-world variability adequately. The modeled variability is used as the null hypothesis for explaining trends, and if it is underestimated (overestimated) this makes it too easy (difficult) to detect significant trends and too difficult (easy) for model simulations to be consistent with observations (Knutson et al. 2013). Therefore, we evaluated the decadal variability of temperature anomalies over the Niño-4 region by comparing a derived observed variability with CMIP5 control run variability. Variability comparisons for other regions have been previously summarized in Knutson et al. (2013), and plots similar to Fig. 2.2e for global temperature and the southern India/Sri Lanka region are shown in the supplemental material.

To isolate the decadal variability, we apply a low-pass filter with a half-power point at nine years. For the observed internal variability temperature estimate, we subtracted the grand ensemble mean of the CMIP5–ALL runs from observations to attempt to remove the forced component of the observed variations. We have not adjusted the forced component estimate to better fit the observations as done in Mann et al. (2014) and Steinmann et al. (2015), which would be a further refinement beyond the scope of this study. As a sensitivity test for Niño-4, we compared the modeled variability (8 GCMs shown in Fig. 2.2e and 23 GCMs in the Supplemental Materials) with that estimated from three different observational datasets. To estimate the model internal variability, we compute the temperature anomaly variance using each model's entire control run. Details for these calculations, and control run lengths used, are described in Knutson et al. (2013). The eight GCM control runs show a wide range of the simulated decadal variances, between 0.025° and 0.08°C^2. The analogous estimates of the unforced component of the variance from the observational reanalyses are 0.048°C^2 (ERSST.v4) and 0.051°C^2 (HadCRUT4v4), both of which are located near the center of the intermodel histogram of the control run decadal variances, while the HadISST1.1 shows a somewhat larger decadal variance (0.068°C^2) which is greater than that from five of the eight models. The sensitivity tests for observed decadal variances, and our earlier sliding trend analyses, indicate that for the Niño-4 region, observational uncertainties significantly obscure the detection and attribution of past trends or recent extreme events.

Conclusions. For 2015, the tendency for a greater ratio of global area covered by extreme annual-mean warm versus cold events, as seen in recent decades, has continued. According to the CMIP5 models, the *risk* of events exceeding the extreme (first- or second-ranked) thresholds for the globe, the Niño-4 region, and southern India/Sri Lanka is almost entirely attributable to anthropogenic forcing, with the ensemble mean FAR above 0.9, and with strong agreement regarding relatively high FAR estimates among the eight GCMs that provided natural-forcing simulations. The strongest model-based evidence for detectable long-term anthropogenic warming, and the highest confidence in a large fraction of attributable risk, was found for the global mean and southern India/

Sri Lanka (SON). In the Niño-4 region, confidence in long-term trend assessment and in the FAR estimates is limited, due to uncertainties in the observational data and a wide range of simulated decadal variances from the control runs.

ACKNOWLEDGEMENTS. We thank the WCRP's Working Group on Coupled Modeling, participating CMIP5 modeling groups, for making available the CMIP5. This study was partly funded by NOAA grant NA14OAR4320106.

REFERENCES

Huang, B., and Coauthors, 2014: Extended Reconstructed Sea Surface Temperature version 4 (ERSST. v4): Part I. Upgrades and intercomparisons. *J. Climate*, **28**, 911–930, doi:10.1175/JCLI-D-14-00006.1.

Kam, J., T. R. Knutson, F. Zeng, and A. T. Wittenberg, 2015: Record annual-mean warmth over Europe, the northeast Pacific, and the northwest Atlantic during 2014: Assessment of anthropogenic influence [in "Explaining Extreme Events of 2014 from a Climate Perspective"]. *Bull. Amer. Meteor. Soc.*, **96 (12)**, S61–S65, doi:10.1175/BAMS-D-15-00101.1.

Knutson, T. R., F. Zeng, and A. T. Wittenberg, 2013: Multimodel assessment of regional surface temperature trends: CMIP3 and CMIP5 Twentieth Century simulations. *J. Climate*, **26**, 8709–8743, doi:10.1175/JCLI-D-12-00567.1.

——, ——, and ——, 2014: Multimodel assessment of extreme annual-mean warm anomalies during 2013 over regions of Australia and the western tropical Pacific [in "Explaining Extreme Events of 2013 from a Climate Perspective"]. *Bull. Amer. Meteor. Soc.*, **95 (9)**, S26–S30.

Mann, M. E., B. A. Steinman, and S. K. Miller, 2014: On forced temperature changes, internal variability, and the AMO. *Geophys. Res. Lett.*, **41**, 3211–3219, doi:10.1002/2014GL059233.

Morice, C. P., J. J. Kennedy, N. A. Rayner, and P. D. Jones, 2012: Quantifying uncertainties in global and regional temperature change using an ensemble of observational estimates: The HadCRUT4 data set. *J. Geophys. Res.*, **117**, D08101, doi:10.1029/2011JD017187.

Rayner, N. A., D. E. Parker, E. B. Horton, C. K. Folland, L. V. Alexander, D. P. Rowell, E. C. Kent, and A. Kaplan, 2003: Global analyses of sea surface temperature, sea ice, and night marine air temperature since the late nineteenth century. *J. Geophys. Res.*, **108**, 4407, doi:10.1029/2002JD002670.

Steinman, B. A., M. E. Mann, and S. K. Miller, 2015: Atlantic and Pacific multidecadal oscillations and northern hemisphere temperatures. *Science*, **347**, 988–991, doi:10.1126/science.1257856.

Stott, P. A., D. A. Stone, and M. R. Allen, 2004: Human contribution to the European heatwave of 2003. *Nature*, **432**, 610–614, doi:10.1038/nature03089.

Taylor, K. E., R. J. Stouffer, and G. A. Meehl, 2012: An overview of CMIP5 and the experimental design. *Bull. Amer. Meteor. Soc.*, **93**, 485–498, doi:10.1175/BAMS-D-00094.1.

Table 28.1. Summary of Results

ANTHROPOGENIC INFLUENCE ON EVENT			
	INCREASE	**DECREASE**	**NOT FOUND OR UNCERTAIN**
Heat	**Global Temperature** (Ch. 2) **South India & Sri Lanka** (Ch. 2) **Central Europe** (Ch. 11) **Europe** (Ch. 12) **Ethiopia and Southern Africa** (Ch. 15) **N.W. China** (Ch. 19) **W. China** (Ch. 20) **Japan** (Ch. 21) **Indonesia** (Ch. 22) **S. Australia** (Ch. 23) **Australia** (Ch. 24)		**Central Equitorial Pacific** (Ch. 2)
Cold		**Northeastern U.S.** (Ch. 7)	**Mid-South Atlantic U.S.** (Ch. 7) **N. America** (Ch. 8)
Heat & Humidity	**Egypt** (Ch. 14) **India & Pakistan** (Ch. 16)		
Dryness	**Indonesia** (Ch. 22) **Tasmania** (Ch. 25)		
Heavy Precipitation	**China** (Ch. 18)		**Nigeria** (Ch. 13) **India** (Ch. 17)
Sunshine	**United Kingdom** (Ch. 10)		
Drought	**Canada** (Ch. 9) **Ethiopia and Southern Africa** (Ch. 15)		
Tropical Cyclones	**Western North Pacific** (Ch. 26)		
Wildfires	**Alaska** (Ch. 4)		
Sea Ice Extent		**Arctic** (Ch. 27)	
High Tide Floods	**Southeastern U.S.** (Ch. 6)		
Snowpack Drought	**Washington U.S.** (Ch. 5)		
TOTAL	**23**	**2**	**5**

	METHOD USED	Total Events
Heat	Ch. 2: **CMIP5 modeling** Ch. 11: **Observations; weather@home modeling** Ch. 12: **HadGEM3-A modeling** Ch. 15: **CMIP5 modeling** Ch. 19: **CMIP5 modeling with ROF; FAR** Ch. 20: **CMIP5 modeling with ROF; FAR** Ch. 21: **MIROC5-AGCM modeling** Ch. 22: **Observations; CMIP5 modeling** Ch. 23: **weather@home modeling; FAR** Ch. 24: **BoM seasonal forecast attribution system and seasonal forecasts**	12
Cold	Ch. 7: **Observations; CMIP5 modeling** Ch. 8: **AMIP (IFS model) modeling**	3
Heat & Humidity	Ch. 14: **weather@home modeling** Ch. 16: **Non-stationary EV theory; C20C+ Attribution Subproject**	2
Dryness	Ch. 22: **Observations; CMIP5 modeling** Ch. 25: **Observations; Modeling with CMIP5 and weather@home**	2
Heavy Precipitation	Ch. 13: **Observations; Modeling with CAM5.1 and MIROC5** Ch. 17: **Observations; Modeling with weather@home, EC-Earth and CMIP5** Ch. 18: **HadGEM3-A-N216 modeling; FAR**	3
Sunshine	Ch. 10: **Hadley Centre event attribution system built on the high-resolution version of HadGEM3-A**	1
Drought	Ch. 9: **Observations; CMIP5 modeling; Trend and FAR analyses** Ch. 15: **CMIP5 modeling, land surface model simulations, and statistical analyses**	2
Tropical Cyclones	Ch. 26: **GFDL FLOR modeling; FAR**	1
Wildfires	Ch. 4: **WRF-ARW optimized for Alaska with metric of fire risk (BUI) to calculate FAR**	1
Sea Ice Extent	Ch. 27: **OGCM modeling**	1
High Tide Floods	Ch. 6: **Tide-gauge data; Time-dependent EV statistical model**	1
Snowpack Drought	Ch. 5: **Observations; CESM1 modeling**	1
		30

ACRONYMS:

AMIP: Atmospheric Model Intercomparison Project
BoM: Bureau of Meteorology, Australia
BUI: Buildup Index
CAM: Community Atmosphere Model, http:www.cesm.ucar.edu
CESM: Community Earth System Model
CMIP: Coupled Model Intercomparison Project
FAR: Fraction of Attributable Risk
EC-EARTH: https://verc.enes.org/
EV: Extreme Value
GFDL FLOR: Geophysical Fluid Dynamics Laboratory Forecast version Low Ocean Resolution
GHCN: Global Historical Climatology Network
IFS: Integrated Forecast System
MIROC5–AGCM: Model for Interdisciplinary Research on Climate–Atmospheric General Circulation Model
OGCM: Ocean General Circulation Model
ROF: Regularized Optimal Fingerprinting
weather@home: http:www.climateprediction.net/weatherathome
WRF-ARW: Advanced Research (ARW) version of the Weather Research and Forecasting (WRF) model